Accepted Manuscript online: 2021-05-19 Article published online: 2021-08-25

Supramolecular Chirogenesis Engineered by Pt(II)···Pt(II) Metal–Metal Interactions

Chengpeng Wei[a]
Mingyang Liu[a]
Yifei Han[a]
Hua Zhong[a]
Feng Wang*[a]

[a] CAS Key Laboratory of Soft Matter Chemistry, Department of Polymer Science and Engineering, University of Science and Technology of China, Hefei, Anhui 230026 (P. R. of China)
drfwang@ustc.edu.cn

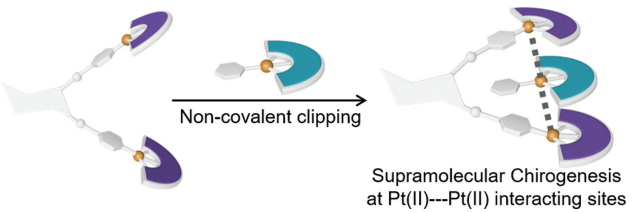

Received: 22.03.2021
Accepted after revision: 16.05.2021
DOI: 10.1055/a-1512-5965; Art ID: om-21-0026sc

Abstract Supramolecular chirogenesis represents an effective way to induce chirality at the supramolecular level. For the previous host–guest chirogenic systems, metal–ligand coordination, hydrogen bonding, π–π stacking and hydrophobic interactions have been mainly employed as the non-covalent driving forces. In this study, Pt(II)···Pt(II) metal–metal interactions have been engineered to induce supramolecular chirogenesis, by forming non-covalent clipping structures between chiral platinum receptors and achiral platinum guests together. This results in the emergence of Cotton effects in the metal–metal-to-ligand charge transfer region, ascribed to chirality transfer from *trans*-1,2-diamide cyclohexane unit on chiral receptors to Pt(II)—Pt(II) non-covalent interacting sites. Supramolecular chirogenesis can be further transferred from organic to aqueous solutions, with higher resistance to concentration and temperature variations in the latter medium. Overall, the current study provides new avenues toward supramolecular chirality systems with tailored properties.

Key words chirality, host–guest recognition, metallotweezers, Pt(II)–Pt(II) metal–metal interactions, supramolecular chemistry

Introduction

Expression of chirality at the supramolecular level is ubiquitous in nature (e.g., the right-handed double helix of DNA), which stimulates the development of artificial supramolecular chirality systems.[1] Up to now, supramolecular chirogenesis has been regarded as an effective way to achieve this goal,[2] which takes place between achiral synthetic receptors and chiral guests (or vice versa) via non-covalent host–guest recognition. The pioneering research in this field was performed by Inoue, Borovkov and coworkers: Upon non-covalent complexation between achiral zinc porphyrin tweezers and chiral amines, circular dichroism (CD) signals were induced in the porphyrin's Soret band region.[3] Later on, a variety of synthetic receptors including molecular tweezers,[4] macrocycles,[5] cages,[6] foldamers,[7] and helical polymers[8] have been utilized for chirogenesis upon complexing the complementary guests. To guarantee specific host–guest complexation in supramolecular chirogenic processes, metal–ligand coordination, hydrogen bonding, π–π stacking, and hydrophobic interactions have been employed individually or conjointly as the non-covalent driving forces. Despite the progresses achieved, new non-covalent forces with effective chirogenic capabilities are required for the further advancement in this field.

To attain this objective, organoplatinum(II) complexes represent an ideal type of supramolecular building blocks.[9] Thanks to the square planar geometry, these compounds show strong tendency to stack with each other in solution and solid states, potentially accompanied by Pt(II)–Pt(II) orbital overlapping between the neighbouring molecules. The so-called Pt(II)–Pt(II) metal–metal interactions[10] result in $5d_z^2$ orbital reorganization into low-lying d_σ and high-lying d_{σ^*} orbitals for the Pt atoms. Further interplay with the ligands leads to the emergence of metal–metal-to-ligand charge transfer (MMLCT) transitions, which commonly located in low-energy visible/NIR region for the absorbance and emission signals. By taking advantage of these fascinating properties, Yam's group has developed label-free sensing techniques toward enzymes and other biologically active molecules, by modulating the strength of Pt(II)–Pt(II) metal–metal interactions with obvious MMLCT spectroscopic changes before/after addition of the analytes.[11] Chi's group has developed high-performance near-infrared organic light-emitting diodes on the basis of MMLCT emission signals in the aggregated state.[12] We envisage that, when Pt(II)···Pt(II) metal–metal interactions are introduced into non-covalent host–guest systems, it facilitates supramolecular chirogenesis in the low-energy MMLCT absorption region. Such unique properties would be especially promising for applications in chiroptical switches and optoelectronic devices.

Recently, our research group has constructed organoplatinum(II)-based supramolecular chirogenic systems via the non-covalent "clipping" effect.[13] Specifically, achiral tweezer receptor and chiral (*R* or *S*)-pinene-substituted platinum(II) guests have been designed to recognize with each other. The resulting host–guest complexes induced Cotton effects, which were driven by Pt(II)···Pt(II) metal–metal and donor–acceptor π–π stacking interactions. To prove the versatility of the "clipping" strategy, herein a vice versa design has been proposed, which contains the chiral Pt(II) receptors (*SS*)-**1** [or (*RR*)-**1**] and achiral guest **2** (Scheme 1). Upon mixing the two compounds together in chloroform, two-fold metal–metal interactions are involved in the non-covalent complexation structures. This results in chirality transfer from the *trans*-1,2-diamide cyclohexane unit on (*SS*)-**1** [or (*RR*)-**1**] to the non-covalent Pt(II)—Pt(II) interacting sites, thus enabling supramolecular chirogenesis in the low-energy MMLCT region. Moreover, the chirogenic behaviours can be transferred from organic to aqueous media, by employing **3** (Scheme 1) as the complementary guest instead of **2**. The current study opens up new avenues toward supramolecular chirogenesis via the elaborate manipulation of non-covalent driving forces.

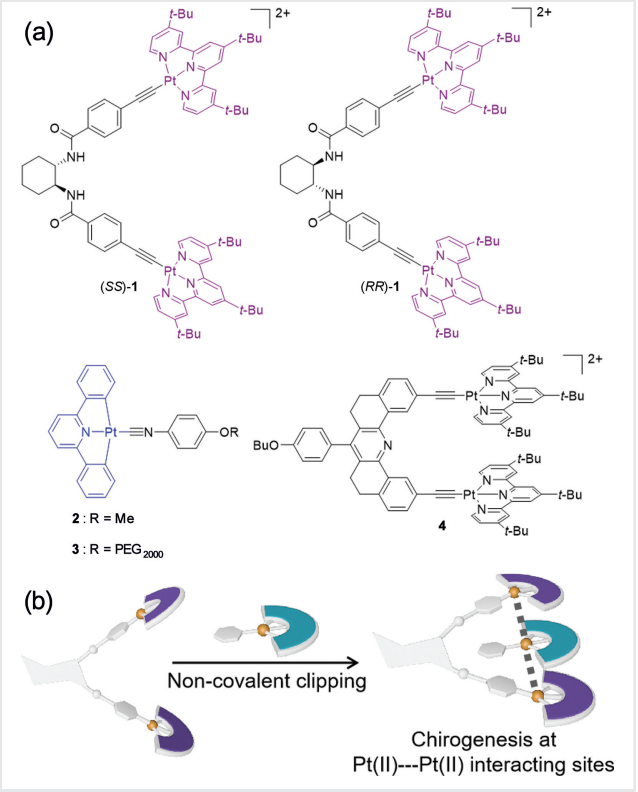

Scheme 1 (a) Chemical structures of chiral Pt(II) receptors (*SS*)-**1**, (*RR*)-**1**, achiral guests **2** and **3**, as well as the control compound **4**. In the chemical structures of (*SS*)-**1**, (*RR*)-**1** and **4**, the counteranions are tetrafluoroborate (BF_4-). (b) Schematic representation for noncovalent complexation between chiral receptors (*SS*)-**1** [or (*RR*)-**1**] and achiral guests **2** (or **3**), which give rise to supramolecular chirogenesis engineered by Pt(II)···Pt(II) metal–metal interactions.

Results and Discussion

Synthesis and Spectroscopy of (*SS*)-1 and (*RR*)-1

The designed compounds (*SS*)-**1** and (*RR*)-**1** were synthesized via copper(I)-catalyzed coupling reactions between chloroplatinum(II) terpyridine and the corresponding bis-acetylene intermediates (Scheme S1).[14,15] The proposed structures were characterized via ^1H, ^{13}C NMR and ESI-MS spectra (Figures S16–S25). In the ^1H NMR spectrum of (*SS*)-**1** (c = 2.00 mM in chloroform), the amide resonances located at 6.86 ppm, while the terpyridine protons $H_{1\text{-}4}$ appeared at 9.10, 7.60, 8.73 and 8.84 ppm, respectively (Figure S1). These aromatic resonances exhibited slight changes upon varying the concentration of (*SS*)-**1** from 0.50 to 10.0 mM (δ for protons H_1: from 9.11 to 9.06 ppm, Figure S1), denoting weak self-association tendency of (*SS*)-**1** (Figure S1).

For UV-Vis spectrum of (*SS*)-**1** ($c = 2 \times 10^{-5}$ M in $CHCl_3$, 298 K, Figure 1a), an intense UV absorbance appeared between 255 and 365 nm ($\varepsilon = 7.73 \times 10^4$ L mol^{-1} cm^{-1} at 286 nm), while a broad absorption band existed between 365 and 490 nm ($\varepsilon = 9.21 \times 10^3$ L mol^{-1} cm^{-1} at 410 nm). With reference to previous literatures,[16] the former band is assigned to the intra-ligand (IL) transitions, while the latter band belongs to the admixture of π(C≡CR)→π*(^{t}Bu$_3$tpy) LLCT (ligand-to-ligand charge transfer) and dπ(Pt)→π* (^{t}Bu$_3$tpy) MLCT (metal-to-ligand charge transfer) transitions. For the emission signals of MLCT/LLCT bands, they were centred at 600 nm upon light excitation at 450 nm (Figure S4). An obvious Cotton effect was observed in the IL absorption region of (*SS*)-**1** (Figure 1b), with a positive maximum at 301 nm ($\Delta\varepsilon$ = +57.7 L mol^{-1} cm^{-1}, g = +-9.88 × 10^{-4}) and a negative one at 275 nm ($\Delta\varepsilon$ = −32.3 L mol^{-1} cm^{-1}, g = −4.58 × 10^{-4}). The Cotton effect in the MLCT/LLCT region was very weak at 2 × 10^{-5} M (Figure 1b), which strengthened upon increasing the concentration to

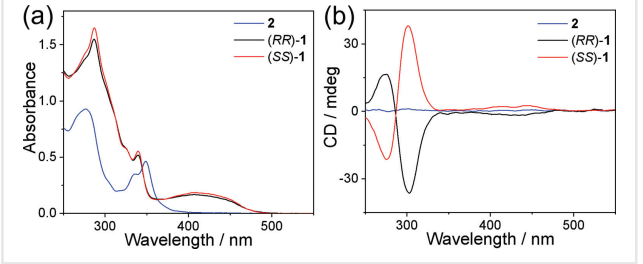

Figure 1 (a) UV-Vis absorption and (b) CD spectra ($CHCl_3$, 0.02 mM) of compounds (*RR*)-**1** (black lines), (*SS*)-**1** (red lines) and **2** (blue lines).

1×10^{-3} M (432 nm; $\Delta\varepsilon = +3.24$ L mol^{-1} cm^{-1}, Figure 5). As expected, the enantiomer compound (*RR*)-**1** displayed the same absorption and mirror-imaged CD signals (Figure 1a, b). The Cotton effects in (*SS*)-**1** and (*RR*)-**1** are ascribed to intrinsic molecular chirality, as validated by the maintenance of CD signals upon elevating the temperature (Figure S2).

Non-covalent Complexation between (*SS*)-/(*RR*)-1 and 2

Upon mixing (*SS*)-**1** and the neutral Pt(II) compound **2** together in $CDCl_3$, the aromatic ^{1}H NMR resonances became broadened and ill-defined, suggesting non-covalent complexation between (*SS*)-**1** and **2** (Figure S3). Absorption and emission spectroscopies were further employed to characterize the resulting non-covalent complexes. For **2** itself, the IL absorption band located below 390 nm (Figure 1a), while no emission signals were observed (Figure S4). For a 1:1 mixture of (*SS*)-**1** and **2** ($c = 1 \times 10^{-3}$ M for each compound in chloroform, 298 K), a new absorption band appeared in the low-energy region (ranging between 510 and 660 nm, $\varepsilon = 2.29 \times 10^3$ L mol^{-1} cm^{-1} at 560 nm, Figure 2a). In the meantime, an emission band emerged in the near-infrared region ($\lambda_{max} = 800$ nm, Figure S4). According to the previous literatures,[17] these emergent spectroscopic signals are characteristic for MMLCT transitions, suggesting the proximity of Pt(II) atoms upon (*SS*)-**1**/**2** non-covalent complexation to induce Pt(II)—Pt(II) metal–metal interactions.

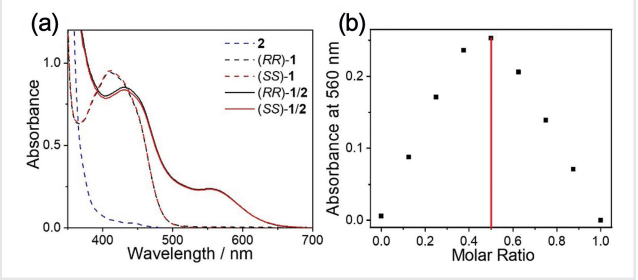

Figure 2 (a) UV-Vis spectra ($CHCl_3$, 1 mM for each of the component) of **2** (blue dash line), (*SS*)-**1** (red dash line), (*RR*)-**1** (black dash line), complexes (*SS*)-**1**/**2** (red solid line) and (*RR*)-**1**/**2** (black solid line). (b) Job's plot of complex (*SS*)-**1**/**2** on the basis of UV-Vis experiments.

Depending on dynamic light scattering (DLS) experiments, no large-sized aggregates were formed for the mixture of (*SS*)-**1** and **2** in chloroform (hydrodynamic diameter: <6 nm, Figure S5b). The result suggests the formation of a discrete supramolecular entity rather than long-range-ordered nanostructures. Notably, George's group has previously reported that, when two π-conjugated chromophores [such as naphthalene diimide and 1-cyano-1,2-bis(phenyl)ethene] are attached to the *trans*-1,2-diamide cyclohexane scaffold, the resulting compounds tend to form large-sized supramolecular polymers as driven by intermolecular hydrogen bonding and π–π stacking interactions.[18] It should be mentioned that difference between the current and George's reported systems lies in the solvents employed. As widely documented, aliphatic solvents such as methylcyclohexane (employed in George's systems) are regarded as the "bad" solvents.[19] They favour hydrogen bonding and π–π stacking interactions, and thereby trigger intermolecular packing to form long-range-ordered nanostructures. In sharp contrast, herein the chlorinated solvent is employed, which is well known as the "good" solvent to prevent aggregation of π-conjugated systems.

To elucidate the exact structural information of non-covalent complexes, we resorted to DFT (density functional theory) calculations. For the optimized geometry of (*SS*)-**1**/**2** (Figure 3b), **2** is sandwiched between the two platinum terpyridine pincers in (*SS*)-**1**, with the inter-planar distances of 3.36 and 3.37 Å, respectively. Notably, the two platinum (II) terpyridine pincers on (*SS*)-**1** are substantially compressed upon sandwiching **2**: the two platinum(II) terpyridine pincers for (*SS*)-**1** itself distort from each other to form a V-shape structure (Pt–Pt distance: 17.7 Å, Figure 3a). Upon encapsulating the complementary guest, the two platinum(II) terpyridine pincers twist closely

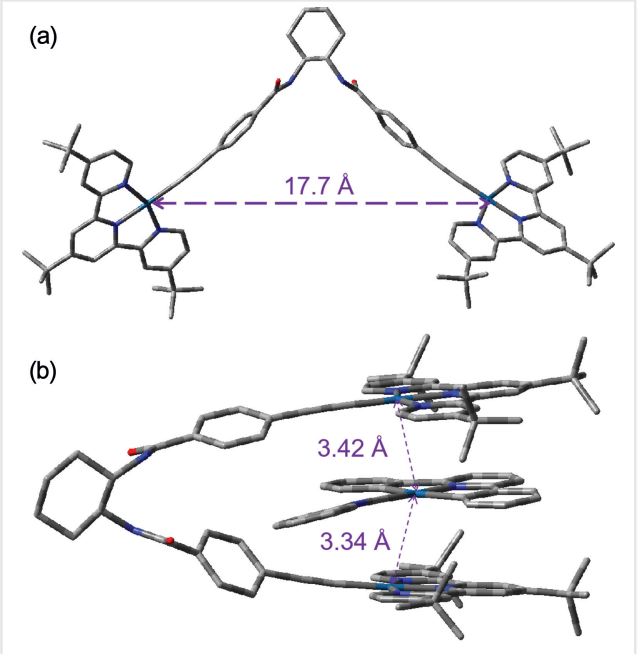

Figure 3 The optimized geometries of (a) (*SS*)-**1** and (b) (*SS*)-**1**/**2** via DFT computation.

[Pt–Pt distance on (*SS*)-**1**: 6.59 Å], which facilitates the generation of donor–acceptor π-stacking interactions toward **2**. More intriguingly, Pt^{2+}—Pt^{2+} distances between two platinum(II) terpyridine pincers on (*SS*)-**1** and **2** were determined to be 3.42 and 3.34 Å, with the Pt—Pt—Pt angle of 153.6°. This unambiguously supports the presence of two-fold Pt(II)—Pt(II) metal–metal interactions in (*SS*)-**1/2**. Hence, (*SS*)-**1** serves as the tweezer receptor and leads to the formation of non-covalent clipping structure (*SS*)-**1/2**. We rationalized that the enthalpy preference upon non-covalent (*SS*)-**1/2** complexation compensates for the loss of conformational entropy in (*SS*)-**1**. The calculation result was verified by means of UV-Vis Job's plot experiments. As shown in Figure 2b, the MMLCT absorbance intensity reaches the maximum value at the equivalent ratio, illustrating 1:1 binding stoichiometry between (*SS*)-**1** and **2**.

Binding Thermodynamics for Complexes (*SS*)-1/2 and (*RR*)-1/2

Non-covalent binding thermodynamics of complex (*SS*)-**1**/**2** was further acquired. With the progressive addition of **2** to (*SS*)-**1**, the MMLCT emission band increased for the intensity, while the MLCT/LLCT emission band of (*SS*)-**1** declined (Figure 4a). Treatment of the collected MLCT/LLCT emission data at 600 nm with a nonlinear curve-fitting equation provided the K_a value of 1.35×10^4 M^{-1} (±6%) for complex (*SS*)-**1**/**2** (Figure 4b). A comparable K_a value was obtained on the basis of ^{1}H NMR titration experiments [$K_a = 1.20 \times 10^4$ M^{-1} (±14%), Figure S6]. In terms of complex (*RR*)-**1**/**2**, the similar K_a value was determined to be 1.46×10^4 M^{-1} (±5%) on the basis of emission measurements (Figure S7).

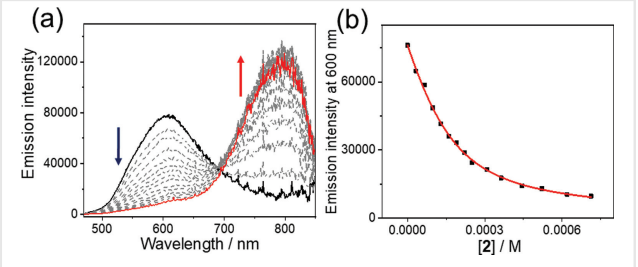

Figure 4 (a) Partial emission signal changes upon gradual addition of **2** into (*SS*)-**1** ($CHCl_3$, 0.20 mM). The arrows indicate the spectral change upon increasing the amount of **2**. (b) Intensity changes of emission intensity at 600 nm, together with the non-linear curve fitting (red line).

As previously reported by us,[16b] the tweezer receptor **4** (Scheme 1) with conformationally rigid spacer is also capable of sandwiching guest **2** into its cavity. As compared to that of complex (*SS*)-**1/2**, the binding affinity of complex **4/2** ($K_a = 7.00 \times 10^4$ M^{-1})[16b] is four times higher. Considering that both receptors **4** and (*SS*)-**1** possess the same platinum terpyridine pincers, it is apparent that the spacer units on tweezer receptors exert crucial impact on the non-covalent binding thermodynamics. In terms of (*SS*)-**1**, the conformational twist for the *trans*-1,2-diamide cyclohexane spacer brings extra entropy loss during the non-covalent complexation process. Meanwhile, the two platinum terpyridine pincers on (*SS*)-**1** are not co-facial with each other in complex (*SS*)-**1**/**2**. Accordingly, it gives rise to weaker π–π/Pt(II)—Pt(II) complexation strengths when comparing to those of complex **4**/**2**.

Supramolecular Chirogenesis for Complexes (*SS*)-1/2 and (*RR*)-1/2

Next, we performed CD spectroscopy for the non-covalent clipping structures. When achiral guest **2** was added into (*SS*)-**1** ($c = 1 \times 10^{-3}$ M for each compound in $CHCl_3$, 298 K), CD intensity in the MCLT/LLCT region (below 490 nm) amplified when compared to that of (*SS*)-**1** (Figure 5). The phenomenon is probably ascribed to the prevention of free bond rotations upon (*SS*)-**1**/**2** complexation. Simultaneously, an obvious Cotton effect emerged in the MMLCT absorption region (between 490 and 650 nm, Figure 5), suggesting chirality transfer from *trans*-1,2-diamide cyclohexane to the non-covalent Pt(II)—Pt(II) interacting sites. Unlike (*SS*)-**1**, the CD signals of complex (*SS*)-**1**/**2** were highly bisignated. In particular, the negative maxima were located at 386 nm ($\Delta\varepsilon = -5.43$ L mol^{-1} cm^{-1}) and 495 nm ($\Delta\varepsilon = -5.22$ L mol^{-1} cm^{-1}), while

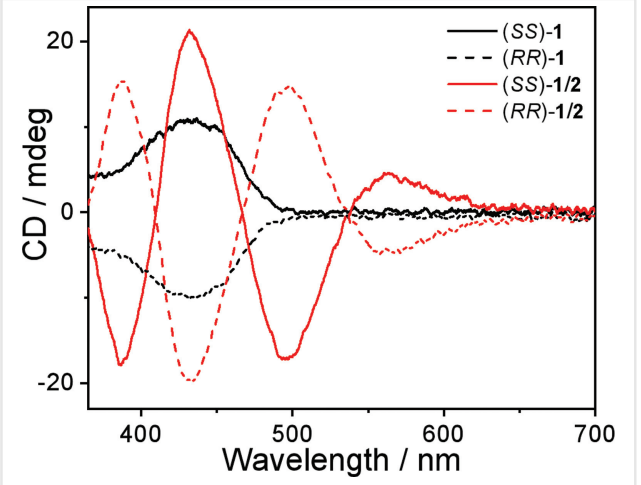

Figure 5 CD spectra (1.00 mM in chloroform) of (*RR*)-**1** (black dash line), (*SS*)-**1** (black dash line), complexes (*RR*)-**1**/**2** (red dash line) and (*SS*)-**1**/**2** (red solid line).

the positive ones at 432 nm ($\Delta\varepsilon = +6.47$ L mol^{-1} cm^{-1}) and 560 nm ($\Delta\varepsilon = +1.40$ L mol^{-1} cm^{-1}). Mirror-image CD spectrum was observed for the enantiomer complex (*RR*)-**1/2** (Figure 5). Accordingly, supramolecular chirogenesis occurred for complexes (*SS*)-**1/2** and (*RR*)-**1/2** in the MMLCT absorption region, which have been seldom encountered for the previous Pt(II)-based supramolecular systems.[20]

Notably, no supramolecular chirogenesis took place for both complexes (*SS*)-**1/2** and (*RR*)-**1/2** at the concentration of 1×10^{-4} M (Figure S8). Considering that (*SS*)-**1/2** [or (*RR*)-**1/2**] are in dynamic equilibrium between complexed and uncomplexed states, we resorted to mathematical calculation to elucidate the concentration-dependent supramolecular chirogenic behaviours. Briefly, when the concentration reaches 1×10^{-3} M^{-1}, 58.1% exists in the complexed (*SS*)-**1/2** form, which acts as the active species toward supramolecular chirogenesis. In stark contrast, the complexed species accounts for 20.7% upon decreasing the concentration to 1×10^{-4} M^{-1}. Hence, non-covalent clipping between (*SS*)-**1** and **2** is a prerequisite for supramolecular chirogenic behaviors.

In addition, supramolecular chirogenesis is highly temperature-dependent. For the 1,2-dichloroethane solution of (*SS*)-**1/2** ($c = 1 \times 10^{-3}$ M for each compound), the CD intensity in the MMLCT region declined upon elevating the temperature, and almost disappeared at 353 K (Figure S9a). The resultant CD signal resembled that of the individual compound (*SS*)-**1**. Break-up of supramolecular chirogenesis is highly plausible, since non-covalent clipping structures dissociated at high temperatures. Upon further cooling to 293 K, the Cotton effects in the MMLCT region fully restored (Figure S9b), validating the reversibility of supramolecular chirogenic signals.

Chiral Amplification for Complexes (*SS*)-1/3 and (*RR*)-1/3 in Water

Water is a green and environmentally friendly medium, which stimulates us to induce supramolecular chirogenesis in aqueous solution. To guarantee sufficient water solubility of the non-covalent clipping structures, poly(ethylene glycol) (PEG_{2000}) was further attached to the guest structure (compound **3**). Similar to that of **2**, **3** was encapsulated into the cavity of (*SS*)-**1** in the chlorinated solvents. It was accompanied by the emergence of MMLCT absorption and CD signals at the concentration of 1×10^{-3} M (Figure S10). Depending on emission titration experiments (Figure S11), the K_a value for the resulting complex (*SS*)-**1/3** in $CHCl_3$ was determined to be 2.31×10^4 M^{-1} ($\pm$ 11%). It is comparable to that of (*SS*)-**1/2**, illustrating the minor impact of the PEG chain on the non-covalent complexation strength.

CD spectroscopy was further performed for (*SS*)-**1/3** in water. In the MMLCT absorption region, the maximum

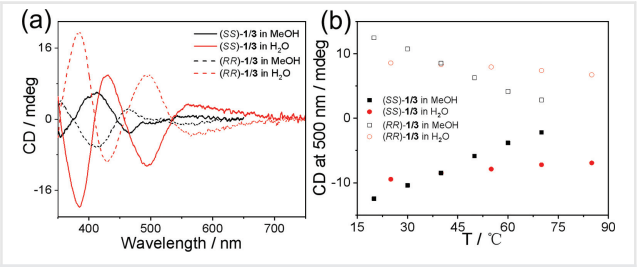

Figure 6 (a) CD spectra (0.10 mM, 298 K) of (*SS*)-**1/3** in methanol (black solid line) and water (red solid line), together with (*RR*)-**1/3** in methanol (black dash line) and water (red dash line). (b) CD intensities at 500 nm (1.00 mM) of complexes (*SS*)-**1/3** and (*RR*)-**1/3** at different temperatures.

positive and negative CD signals appeared at 579 nm ($\Delta\varepsilon = +2.40$ L mol^{-1} cm^{-1}) and 499 nm ($\Delta\varepsilon = -2.88$ L mol^{-1} cm^{-1}) for 1.00×10^{-3} M aqueous solution of (*SS*)-**1/3**, respectively (Figure S12). Remarkably, supramolecular chirogenic signals in water are more resistant to concentration variations, as reflected by the maintenance of Cotton effects at a low concentration (1.0×10^{-4} M, Figure 6a). It is contrary to the aforementioned results in organic media, which lost supramolecular chirality and displayed molecular chirality signals. The improved chirogenic phenomenon originates from supramolecular assembly of (*SS*)-**1/3** in water, because of phase segregation between hydrophobic tweezer/guest complex and hydrophilic PEG_{2000} chains (Figure S13a). The conclusion was validated by means of DLS measurements: the hydrodynamic diameters of (*SS*)-**1/3** increased from 6 to 76 nm upon switching the solvent from methanol to water (Figure S13b). According to transmission electron microscopy (TEM) measurements, complex (*SS*)-**1/3** was prone to form nanoparticles with the averaged diameter of 200 nm in water (Figure S13c). The larger diameters in TEM could be ascribed to the existence of molecule–surface interactions when depositing supramolecular aggregates of (*SS*)-**1/3** on the solid support. Additional evidence for the assembly of (*SS*)-**1/3** came from solvent-dependent UV-Vis measurements, which displayed an isosbestic point at 562 nm upon varying the methanol/water volume ratio (from 10.0% to 38.3%, Figure S14). Benefited from this, the supramolecular chirogenic signals of (*SS*)-**1/3** maintained at elevated temperatures (at 495 nm: $\Delta\varepsilon = |2.21|$ L mol^{-1} cm^{-1} at 358 K vs. |2.80| L mol^{-1} cm^{-1} at 298 K; Figures 6b and S15).

Conclusions

In summary, herein supramolecular chirogenic systems engineered by Pt(II)···Pt(II) metal–metal interactions have been successfully constructed. The key design principle is non-covalent recognition between chiral receptors (*SS*)-**1**

[or (*RR*)-**1**] and achiral guest **2**, giving rise to the formation of clipping complexes (*SS*)-**1/2** [or (*RR*)-**1/2**] with two-fold π–π stacking and Pt(II)···Pt(II) metal–metal bonds. Cotton effects emerged in the low-energy MMLCT region, thanks to chirality transfer from the *trans*-1,2-diamide cyclohexane unit on (*SS*)-**1** [or (*RR*)-**1**] to the Pt(II)—Pt(II) interacting sites. For complex (*SS*)-**1**/**3**, the attachment of a PEG2000 unit enables supramolecular chirogenesis in water. More importantly, assembly of (*SS*)-**1**/**3** leads to the high resistance of supramolecular chirogenic signals toward concentration and temperature variations. Overall, with the elaborate manipulation of non-covalent driving forces, the current study provides new avenues toward supramolecular chiral systems with tailored properties.

Funding Information

This work was supported by the National Natural Science Foundation of China (21922110 and 21871245), the Fundamental Research Funds for the Central Universities (WK3450000005), and the CAS Youth Innovation Promotion Association (Y201986). The DFT computations were performed at the supercomputing center. We are grateful for the technical support from the High-Performance Computing Center of the University of Science and Technology of China.

Supporting Information

Supporting Information for this article is available online at https://doi.org/10.1055/a-1512-5965.

References and Notes

(1) (a) Yashima, E.; Ousaka, N.; Taura, D.; Shimomura, K.; Ikai, T.; Maeda, K. *Chem. Rev.* **2016**, *116*, 13752. (b) Liu, M.; Zhang, L.; Wang, T. *Chem. Rev.* **2015**, *115*, 7304. (c) Palmans, A. R. A.; Meijer, E. W. *Angew. Chem. Int. Ed.* **2007**, *46*, 8948. (d) Dorca, Y.; Greciano, E. E.; Valera, J. S.; Gómez, R.; Sánchez, L. *Chem. Eur. J.* **2019**, *25*, 5848.

(2) (a) Borovkov, V. V.; Hembury, G. A.; Inoue, Y. *Acc. Chem. Res.* **2004**, *37*, 449. (b) Bobadilla, M. V. E.; Kleij, A. W. *Chem. Sci.* **2012**, *3*, 2421. (c) Dhamija, A.; Mondal, P.; Saha, B. *Dalton Trans.* **2020**, *49*, 10679.

(3) Borovkov, V. V.; Lintuluoto, J. M.; Inoue, Y. *J. Am. Chem. Soc.* **2001**, *123*, 2979.

(4) (a) Brahma, S.; Ikbal, S. A.; Dey, S.; Rath, S. P. *Chem. Commun.* **2012**, *48*, 4070. (b) Brahma, S.; Ikbal, S. A.; Rath, S. P. *Inorg. Chem.* **2014**, *53*, 49. (c) Ikbal, S. A.; Brahma, S.; Rath, S. P. *Chem. Commun.* **2015**, *51*, 895.

(5) (a) Wang, L. L.; Chen, Z.; Liu, W. E.; Ke, H.; Wang, S. H.; Jiang, W. *J. Am. Chem. Soc.* **2017**, *139*, 8436. (b) Zhu, H.; Li, Q.; Gao, Z.; Wang, H.; Shi, B.; Wu, Y.; Shangguan, L.; Hong, X.; Wang, F.; Huang, F. *Angew. Chem. Int. Ed.* **2020**, *59*, 10868. (c) Chai, H.; Chen, Z.; Wang, S.-H.; Quan, M.; Yang, L.-P.; Ke, H.; Jian, W. *CCS Chem.* **2020**, *2*, 440.

(6) (a) Rizzuto, F. J.; Pröhm, P.; Plajer, A. J.; Greenfield, J. L.; Nitschke, J. R. *J. Am. Chem. Soc.* **2019**, *141*, 1707. (b) Li, B.; Zheng, B.; Zhang, W.; Zhang, D.; Yang, X. J.; Wu, B. *J. Am. Chem. Soc.* **2020**, *142*, 6304.

(7) (a) Korevaar, P. A.; George, S. J.; Markvoort, A. J.; Smulders, M. M.; Hilbers, P. A. J.; Schenning, A. P. H. J.; De Greef, T. F.; Meijer, E. W. *Nature* **2012**, *481*, 492. (b) Dolain, C.; Jiang, H.; Léger, J. M.; Guionneau, P.; Huc, I. *J. Am. Chem. Soc.* **2005**, *127*, 12943. (c) George, S. J.; Tomović, Z.; Smulders, M. M. J.; de Greef, T. F. A.; Leclère, P. E. L. G.; Meijer, E. W.; Schenning, A. P. H. J. *Angew. Chem. Int. Ed.* **2007**, *46*, 8206.

(8) (a) Greenfield, J. L.; Evans, E. W.; Di Nuzzo, D.; Di Antonio, M.; Friend, R. H.; Nitschke, J. R. *J. Am. Chem. Soc.* **2018**, *140*, 10344. (b) Ishikawa, M.; Maeda, K.; Yashima, E. *J. Am. Chem. Soc.* **2002**, *124*, 7448. (c) Yashima, E.; Maeda, K.; Furusho, Y. *Acc. Chem. Res.* **2008**, *41*, 1166.

(9) (a) Mauro, M.; Aliprandi, A.; Septiadi, D.; Kehr, N. S.; De Cola, L. *Chem. Soc. Rev.* **2014**, *43*, 4144. (b) Yoshida, M.; Kato, M. *Coord. Chem. Rev.* **2020**, *408*, 213194. (c) Herkert, L.; Sampedro, A.; Fernández, G. *CrystEngComm* **2016**, *18*, 8813. (d) Yam, V. W.-W.; Au, V. K.-M.; Leung, S. Y.-L. *Chem. Rev.* **2015**, *115*, 7589. (e) Crowley, J. D.; Steele, I. M.; Bosnich, B. *Inorg. Chem.* **2005**, *44*, 2989. (f) Crowley, J. D.; Steele, I. M.; Bosnich, B. *Eur. J. Inorg. Chem.* **2005**, 3907.

(10) (a) Wong, K. M.-C.; Yam, V. W.-W. *Acc. Chem. Res.* **2011**, *44*, 424. (b) Gao, Z.; Han, Y.; Gao, Z.; Wang, F. *Acc. Chem. Res.* **2018**, *51*, 2719. (c) Han, Y.; Gao, Z.; Wang, C.; Zhong, R.; Wang, F. *Coord. Chem. Rev.* **2020**, *414*, 213300.

(11) (a) Chung, C. Y.-S.; Yam, V. W.-W. *J. Am. Chem. Soc.* **2011**, *133*, 18775. (b) Wong, K. M.-C.; Chan, M. M.-Y.; Yam, V. W.-W. *Adv. Mater.* **2014**, *26*, 5558. (c) Chung, C. Y.-S.; Chan, K. H.; Yam, V. W.-W. *Chem. Commun.* **2011**, *47*, 2000. (d) Chung, C. Y.-S.; Yam, V. W.-W. *Chem. Sci.* **2013**, *4*, 377. (e) Chan, M. C.-L.; Yam, V. W.-W. *Chem. Eur. J.* **2011**, *17*, 11987.

(12) (a) Ly, K. T.; Cheng, R. W. C.; Lin, H. W.; Shiau, Y. J.; Liu, S. H.; Chou, P. T.; Tsao, C. S.; Huang, Y. C.; Chi, Y. *Nat. Photonics* **2017**, *11*, 63. (b) Chen, W. C.; Sukpattanacharoen, C.; Chan, W. H.; Huang, C. C.; Hsu, H. F.; Shen, D.; Hung, W. Y.; Kungwan, N.; Escudero, D.; Lee, C. S.; Chi, Y. *Adv. Funct. Mater.* **2020**, *30*, 2002494.

(13) (a) Liu, M.; Han, Y.; Zhong, H.; Zhang, X.; Wang, F. *Angew. Chem. Int. Ed.* **2021**, *60*, 3498. (b) Li, Z.; Han, Y.; Nie, F.; Liu, M.; Zhong, H.; Wang, F. *Angew. Chem. Int. Ed.* **2021**, *60*, 8212. (c) Tian, Y.-K.; Shi, Y.-G.; Yang, Z.-S.; Wang, F. *Angew. Chem. Int. Ed.* **2014**, *53*, 6090. (d) Tian, Y.-K.; Han, Y.-F.; Yang, Z.-S.; Wang, F. *Macromolecules* **2016**, *49*, 6455. (e) Zhang, X.; Han, Y.; Liu, G.; Wang, F. *Chin. Chem. Lett.* **2019**, *30*, 1927.

(14) **Synthetic procedure for compound (*SS*)-1:** Compound (*SS*)-**5** (30.0 mg, 0.08 mmol), [Pt(tpy)Cl](BF$_4$) (128 mg, 0.18 mmol), CuI (20.0 mg, 0.10 mmol) and TEA (3 mL) in DMF were stirred under a nitrogen atmosphere at room temperature for 48 hours. The mixture was evaporated under reduced pressure, and the residue was extracted with H_2O/CH_2Cl_2. The combined organic extracts were removed with a rotary evaporator, and the residue was purified by flash column chromatography (CH_2Cl_2/CH_3OH, 50:1 v/v as the eluent; $R_f = 0.3$) to afford (*SS*)-**1** as a yellow solid (120 mg, 86%). ^{1}H NMR (400 MHz, $CDCl_3$) δ: 9.09 (d, J = 6.0 Hz, 4 H), 8.86 (s, 4 H), 8.75 (d, J = 2.1 Hz, 4 H), 7.76–7.69 (m, 4 H), 7.60 (dd, J = 6.1, 2.1 Hz, 4 H), 7.53–7.46 (m, 4 H), 6.91 (s, 2 H), 4.05 (s, 2 H), 2.26 (d, J = 9.6 Hz, 2 H), 1.88 (s, 2 H), 1.66 (s, 18 H), 1.51 (s, 36 H). ^{13}C NMR (101 MHz, $CDCl_3$:CH_3OD = 3:1) δ: 167.4, 166.3,

157.6, 152.8, 152.6, 130.9, 130.8, 130.1, 127.8, 126.0, 124.5, 122.6, 121.0, 51.7, 36.7, 35.6, 30.5, 29.8, 29.3, 28.7. HRMS: *m*/*z*: $[M - 2BF_4]^{2+}$, experimental, 780.3229; calculated, 780.3241, error 1.5 ppm.

(15) **Synthetic procedure for compound (*RR*)-1:** A similar procedure to that of (*SS*)-**1** was adopted, by employing (*RR*)-**5** (250 mg, 2.19 mmol) instead of (*SS*)-**5**. Compound (*RR*)-**1** was obtained as a yellow solid (117 mg, 84%). ^{1}H NMR (400 MHz, $CDCl_3$ δ: 9.09 (d, J = 6.0 Hz, 4 H), 8.68 (s, 4 H), 8.59 (s, 4 H), 7.73 (d, *J* = 7.9 Hz, 4 H), 7.62 (d, *J* = 6.0 Hz, 4 H), 7.49 (d, *J* = 8.0 Hz, 4 H), 6.96–6.88 (m, 2 H), 4.06 (s, 2 H), 2.24 (s, 2 H), 1.88 (s, 2 H), 1.66 (s, 18 H), 1.51 (s, 36 H), 1.47 (s, 4 H). ^{13}C NMR (101 MHz, $CDCl_3$ δ: 166.4, 152.7, 130.8, 126.0, 124.2, 121.4, 53.9, 36.8, 35.6, 29.8, 29.3, 28.3, 28.3. HRMS: *m*/*z*: $[M - 2BF_4]^{2+}$, experimental, 780.3226; calculated, 780.3241, error 1.9 ppm.

(16) (a) Tanaka, Y.; Wong, K. M.-C.; Yam, V. W.-W. *Chem. Sci.* **2012**, *3*, 1185. (b) Li, Z.; Han, Y.; Jin, F.; Gao, Z.; Gao, Z.; Ao, L.; Wang, F. *Dalton Trans.* **2016**, *45*, 17290. (c) Li, Z.; Han, Y.; Gao, Z.; Fu, T.; Wang, F. *Mater. Chem. Front.* **2018**, *2*, 76. (d) Han, Y.; Tian, Y.; Li, Z.; Wang, F. *Chem. Soc. Rev.* **2018**, *47*, 5165. (e) Ibáñez, S.; Poyatos, M.; Peris, E. *Angew. Chem. Int. Ed.* **2017**, *56*, 9786. (f) Biz, C.; Ibáñez, S.; Poyatos, M.; Gusev, D.; Peris, E. *Chem. Eur. J.* **2017**, *23*, 14439. (g) Ibáñez, S.; Poyatos, M.; Peris, E. *Angew. Chem. Int. Ed.* **2018**, *57*, 16816. (h) Ibáñez, S.; Peris, E. *Chem. Eur. J.* **2019**, *25*, 8254.

(17) (a) Leung, S. Y.-L.; Tam, A. Y.-Y.; Tao, C.-H.; Chow, H. S.; Yam, V. W.-W. *J. Am. Chem. Soc.* **2012**, *134*, 1047. (b) Li, Z.; Han, Y.; Gao, Z.; Wang, F. *ACS Catal.* **2017**, *7*, 4676.

(18) (a) Narayan, B.; Bejagam, K. K.; Balasubramanian, S.; George, S. J. *Angew. Chem. Int. Ed.* **2015**, *54*, 13053. (b) Sarkar, S.; Narayan, B.; George, S. J. *ChemNanoMat* **2020**, *6*, 1169.

(19) Chen, Z.; Lohr, A.; Saha-Möller, C. R.; Würthner, F. *Chem. Soc. Rev.* **2009**, *38*, 564.

(20) (a) Leung, S. Y.-L.; Lam, W. H.; Yam, V. W.-W. *Proc. Natl. Acad. Sci. U.S.A.* **2013**, *110*, 7986. (b) Norel, L.; Rudolph, M.; Vanthuyne, N.; Williams, J. A. G.; Lescop, C.; Roussel, C.; Autschbach, J.; Crassous, J.; Réau, R. *Angew. Chem. Int. Ed.* **2010**, *49*, 99. (c) Aliprandi, A.; Croisetu, C. M.; Mauro, M.; Cola, L. *Chem. Eur. J.* **2017**, *23*, 5957. (d) Gao, Z.; Tian, Y.; Hsu, H. K.; Han, Y.; Chan, Y. T.; Wang, F. *CCS Chem.* **2021**, *3*, 105.